ARTICLE

Treatment of hypophosphatasia by muscle-directed expression of bone-targeted alkaline phosphatase via self-complementary AAV8 vector

Aki Nakamura-Takahashi[1], Koichi Miyake[1], Atsushi Watanabe[1,2], Yukihiko Hirai[1], Osamu Iijima[1], Noriko Miyake[1], Kumi Adachi[1], Yuko Nitahara-Kasahara[1], Hideaki Kinoshita[3], Taku Noguchi[4], Shinichi Abe[4], Sonoko Narisawa[5], Jose Luis Millán[5], Takashi Shimada[1] and Takashi Okada[1]

Hypophosphatasia (HPP) is an inherited disease caused by genetic mutations in the gene encoding tissue-nonspecific alkaline phosphatase (TNALP). This results in defects in bone and tooth mineralization. We recently demonstrated that TNALP-deficient (*Akp2*$^{-/-}$) mice, which mimic the phenotype of the severe infantile form of HPP, can be treated by intravenous injection of a recombinant adeno-associated virus (rAAV) expressing bone-targeted TNALP with deca-aspartates at the C-terminus (TNALP-D$_{10}$) driven by the tissue-nonspecific CAG promoter. To develop a safer and more clinically applicable transduction strategy for HPP gene therapy, we constructed a self-complementary type 8 AAV (scAAV8) vector that expresses TNALP-D$_{10}$ via the muscle creatine kinase (MCK) promoter (scAAV8-MCK-TNALP-D$_{10}$) and examined the efficacy of muscle-directed gene therapy. When scAAV8-MCK-TNALP-D$_{10}$ was injected into the bilateral quadriceps of neonatal *Akp2*$^{-/-}$ mice, the treated mice grew well and survived for more than 3 months, with a healthy appearance and normal locomotion. Improved bone architecture, but limited elongation of the long bone, was demonstrated on X-ray images. Micro-CT analysis showed hypomineralization and abnormal architecture of the trabecular bone in the epiphysis. These results suggest that rAAV-mediated, muscle-specific expression of TNALP-D$_{10}$ represents a safe and practical option to treat the severe infantile form of HPP.

Molecular Therapy — Methods & Clinical Development (2016) **3**, 15059; doi:10.1038/mtm.2015.59; published online 3 February 2016

INTRODUCTION

Hypophosphatasia (HPP) is an inherited disease caused by genetic mutations in the gene encoding tissue-nonspecific alkaline phosphatase (TNALP) that results in defects in bone and tooth mineralization.[1] The clinical presentation of HPP is highly variable and ranges from a lethal perinatal form to mild odonto-HPP that is characterized only by dental abnormalities.[2] In cases of infantile HPP, postnatal development appears to proceed normally, but the patients suffer from systemic hypomineralization, respiratory insufficiency, and epileptic seizures, and the disease is often fatal before 6 months of age. Pyridoxine-responsive convulsions frequently occur in severe forms of infantile HPP.[3–5] There is no confirmed standard treatment for HPP, but several experimental approaches have been examined using TNALP knockout (*Akp2*$^{-/-}$) mice, the phenotype of which mimics that of severe infantile HPP. The mice are born with a normal appearance, but they quickly develop growth impairment, epileptic seizures, and hypomineralization, and die within 3 weeks of birth.[6]

Because TNALP is an ectoenzyme that attaches to the outer cell membrane via a glycosylphosphatidylinositol anchor, enzyme replacement therapy (ERT) is considered a viable approach for the treatment of HPP.[1,2] *Akp2*$^{-/-}$ mice can be effectively treated by ERT using bone-targeted TNALP with deca-aspartates at the C-terminus (TNALP-D$_{10}$).[7] Based on this finding, a clinical trial utilizing ERT for the treatment of infantile HPP was initiated as a "breakthrough therapy" in the United States;[8] however, repeated administration of large amounts of costly recombinant enzyme is required to realize therapeutic benefits.

Gene therapy represents a viable alternative for the treatment of HPP. We recently demonstrated that *Akp2*$^{-/-}$ mice can be rescued by a single intravenous injection of recombinant adeno-associated virus (rAAV) expressing TNALP-D$_{10}$ driven by the tissue-nonspecific CAG promoter, a hybrid promoter of the actin gene promoter and the CMV-IE enhancer.[9] This gene therapy strategy is essentially vector-mediated ERT but is less invasive and more cost effective than classical ERT. The potential problem of this approach, however, is the risk of unexpected adverse effects caused by transduction of nontargeted tissues[10] including the gonads. Because the subjects of HPP gene therapy are neonatal patients, the safety of systemic injection of the viral vector must be carefully evaluated before clinical application.

As an alternative approach, we examined the feasibility of muscle-directed gene therapy for HPP. Skeletal muscle is a

[1]Department of Biochemistry and Molecular Biology, Nippon Medical School, Tokyo, Japan; [2]Division of Clinical Genetics, Nippon Medical School Hospital, Tokyo, Japan; [3]Department of Dental Materials Science, Tokyo Dental College, Tokyo, Japan; [4]Department of Anatomy, Tokyo Dental College, Tokyo, Japan; [5]Sanford Children's Health Research Center, Sanford-Burnham Prebys Medical Discovery Institute, La Jolla, California, USA. Correspondence: T Okada (t-okada@nms.ac.jp)

practical target organ for gene therapy because it is easily accessible and has a large capacity for protein production. Direct injection of AAV vector into the muscle has been widely used both for the treatment of muscle disease[11] and for the expression of soluble proteins to treat systemic metabolic disease including lipoprotein lipase deficiency, which is being treated with the first EU-approved AAV type 1 vector (Glybera).[12] In this study, we constructed a self-complementary AAV type 8 (scAAV8) vector that expresses TNALP-D_{10} via the muscle-specific creatine kinase (MCK) promoter (scAAV8-MCK-TNALP-D_{10}) and examined the efficacy of muscle-directed gene therapy.

RESULTS

Muscle-directed transduction with the MCK promoter

To confirm muscle-specific expression by the MCK promoter *in vitro*, C2C12 (a myoblast-like cell line from the C3H mouse), HEK293, or HeLa cells were transduced with scAAV8-MCK-EGFP, or a control vector harboring the chicken beta-actin (CBA) promoter scAAV8-CBA-EGFP. Expression of enhanced green fluorescent protein (EGFP) was visualized with an inverted fluorescent microscope 72 hours after transduction, which revealed a strong expression in the C2C12 cells. Flow cytometry analysis showed that the EGFP expression induced by scAAV8-MCK-EGFP in C2C12 cells ($36.2 \pm 2.0\%$) was higher than that induced in HEK293 ($0.7 \pm 0.2\%$) or HeLa ($3.1 \pm 0.2\%$) cells (see Supplementary Figure S1a). Furthermore, MCK promoter–driven expression of EGFP was normalized on the basis of the CBA promoter–driven expression. As a result, similar tendency was obtained with the normalized numbers (C2C12; 73.9%, HEK293; 1.86%, HeLa; 6.14%, see Supplementary Figure S1b).

Muscle transduction with the MCK promoter was also analyzed *in vivo.* Cryostat tissue sections from the muscle, heart, liver, and kidneys of scAAV8-MCK-EGFP intramuscular (i.m.)-injected mice were analyzed 14 days after transduction. Expression of EGFP by the MCK promoter produced intense fluorescence in the muscle and heart (higher in muscle than in heart) but not in other tissues (see Supplementary Figure S1c). These data suggested that the MCK promoter retained the ability to drive muscle-specific expression.

Sustained expression of TNALP-D_{10} and prolonged survival in scAAV8-MCK-TNALP-D_{10}–injected *Akp2*$^{-/-}$ mice

scAVV8-MCK-TNALP-D_{10} (2.5×10^{12} vector genome (v.g.)/body) was injected into the bilateral quadriceps femoris muscle of neonatal *Akp2*$^{-/-}$ mice on day 1. To measure the TNALP-D_{10} levels in the plasma during the course of muscle transduction, ALP activity was analyzed by colorimetric assay. Plasma ALP activity levels over 1 unit/ml (U/ml) have been shown to prolong survival of *Akp2*$^{-/-}$ mice.[9,13,14] At 30 days after birth, the ALP activity in the plasma of an untreated *Akp2*$^{-/-}$ mouse was 0.05 U/ml ($n = 1$). In contrast, plasma ALP activities of scAAV8-MCK-TNALP-D_{10}–treated *Akp2*$^{-/-}$ (TNALP-D_{10}) mice ($n=9$) were increased by more than 10-fold over those in *Akp2*$^{+/+}$ (wild-type (WT)) mice ($n = 10$) and were sustained throughout the observation period (means $\pm$ SD, TNALP-D_{10} versus WT; 4.92 ± 1.72 versus 0.16 ± 0.046 U/ml on day 30, $P < 0.001$; 1.63 ± 0.56 versus 0.11 ± 0.018 U/ml on day 60, $P < 0.001$; and 1.27 ± 0.69 versus 0.087 ± 0.025 U/ml on day 90, $P < 0.001$ (Figure 1a). As shown in Figure 1b, the life spans of TNALP-D_{10} mice ($n = 9/10$) were significantly prolonged ($P < 0.001$, log-rank test) compared with untreated *Akp2*$^{-/-}$ mice ($n = 9$). These results suggested that muscle-specific TNALP-D_{10} transduction induces therapeutic effects comparable with those observed in our previous study using a nonspecific promoter.
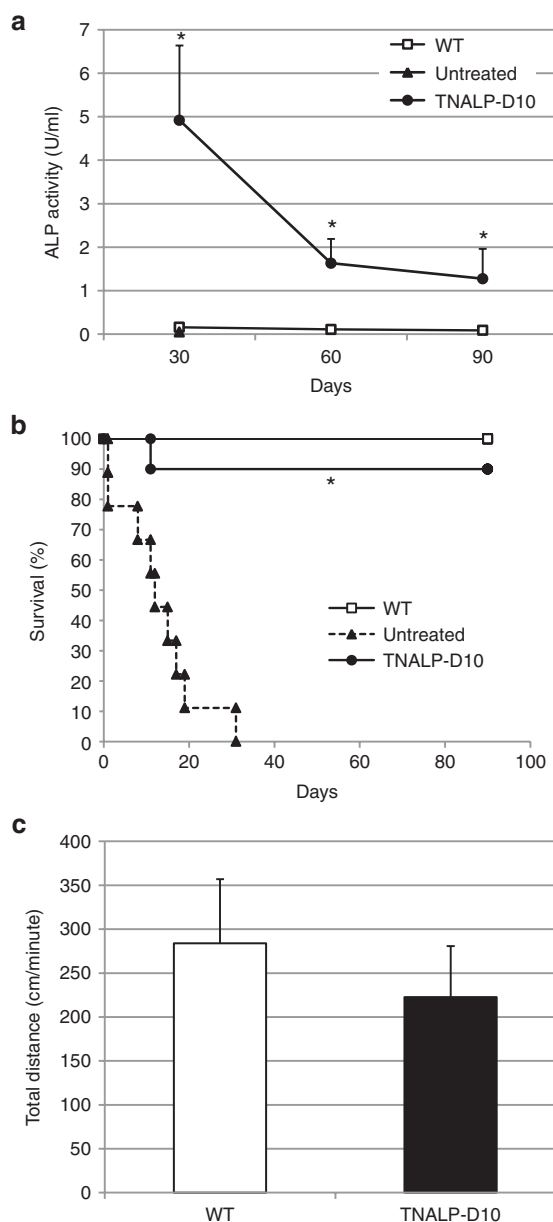

Figure 1 Gene transduction of *Akp2*$^{-/-}$ mice with scAAV8-MCK-TNALP-D_{10} (TNALP-D_{10}). (**a**) Plasma ALP activity in an untreated *Akp2*$^{-/-}$ mouse ($n = 1$), wild-type (WT) mice ($n = 10$), and TNALP-D_{10} mice ($n = 9$). Data represent the means $\pm$ SD. *$P < 0.001$. (**b**) Survival curves of WT mice ($n = 10$), untreated *Akp2*$^{-/-}$ mice ($n = 9$), and TNALP-D_{10} mice ($n = 10$). Data represent the means $\pm$ SD. *$P < 0.001$. (**c**) At 30 days after birth, locomotor activity in WT mice ($n = 5$) and TNALP-D_{10} mice ($n = 7$) given as total distance (cm) covered over a 1-minute period in an open field. MCK, muscle creatine kinase; TNALP-D_{10}, tissue-nonspecific alkaline phosphatase with deca-aspartates at the C-terminus.

scAAV8-MCK-TNALP-D_{10}–treated *Akp2*$^{-/-}$ mice appear healthy with normal levels of physical activity

We first examined the physical activity of the TNALP-D_{10} mice. At postnatal days 6–8, untreated mice exhibited growth impairment, displayed spontaneous seizures as well as apnea, and died within 3 weeks of birth. In contrast, at 30 days after birth, there was no significant difference in total distance traveled between the TNALP-D_{10} mice ($n = 7$) and control WT mice ($n = 5$) in the open field (means $\pm$ SD, TNALP-D_{10} versus WT; 222.7 ± 58.1 cm/minute versus

Targeted treatment of HPP via the MCK promoter
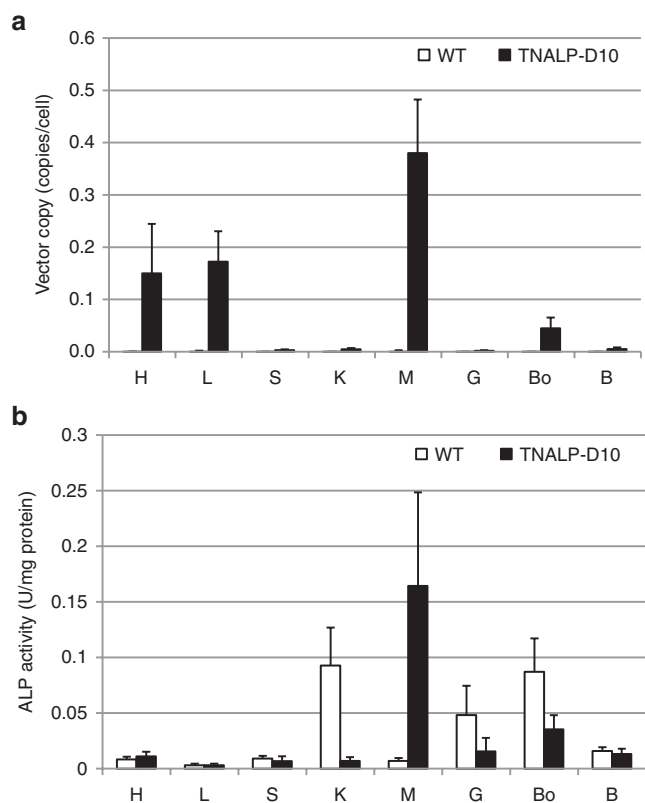A Nakamura-Takahashi *et al*.

npg

3

Figure 2 ALP supplementation following muscle transduction. (**a**) Vector distribution. (**b**) ALP activity in the various tissues of wild-type (WT) mice ($n = 5$) and TNALP-D$_{10}$ mice ($n = 5$). B, brain; Bo, bone and bone marrow; G, genitalia; H, heart; K, kidney; L, liver; M, muscle; S, spleen; TNALP-D$_{10}$, tissue-nonspecific alkaline phosphatase with deca-aspartates at the C-terminus.

284.0 ± 73.0 cm/minute, $P = 0.14$; Figure 1c). In addition, TNALP-D$_{10}$ mice were healthy in appearance and exhibited normal physical activities, including running, jumping, and climbing up the gauge (data not shown).

ALP supplementation with muscle transduction

To determine which organs were the primary sources of supplemented TNALP-D$_{10}$ in the treated mice at 90 days of age, we examined the vector distributions and ALP activities in eight organs from TNALP-D$_{10}$ mice ($n = 5$) or WT mice ($n = 5$). The highest vector copy number was observed in the quadriceps femoris muscle, at the site of AAV vector injection. Lower copy numbers of vector were observed in the heart, liver, and bone and bone marrow. (Figure 2a).

In addition, high-level ALP activity was restricted to the injected muscle tissue (means ± SD, TNALP-D$_{10}$ versus WT; 0.164 ± 0.084 versus 0.007 ± 0.003 U/mg, $P < 0.001$), ALP activity was not remarkable in the heart or the liver, despite vector distribution within those tissues (Figure 2b). Ectopic calcification was not detected at the injection site or in any other organs.

Improved bone formation with limited elongation of the long bone following TNALP-D$_{10}$ transduction

To characterize bone structure in the transduced mice, we performed radiography of the hind limb, foot, forepaw, coccygeal vertebrae, and thorax in day 90 TNALP-D$_{10}$ mice ($n = 9$) and WT mice ($n = 5$).

Untreated *Akp2*$^{-/-}$ mice appeared normal at birth, but radiographic changes were apparent by 20 days after birth. Compared with WT mice, the bones of untreated *Akp2*$^{-/-}$ mice demonstrated hypomineralization, shortened femurs, and increased spaces between adjacent coccygeal vertebrae (see Supplementary Figure S2a).

Conversely, WT and TNALP-D$_{10}$ mice exhibited normal skeletal structure and mineralization of the thorax, forepaw, and foot (Figure 3a,b,c). The hind limbs of day 90 TNALP-D$_{10}$ mice were normal in appearance, although the femur lengths were shorter than those in WT mice (Figure 3d,e; $P < 0.01$). Similarly, the coccygeal vertebrae of the day 90 TNALP-D$_{10}$ mice exhibited reduced intervertebral spaces but were significantly wider than those of the WT mice (Figure 3f,g; $P < 0.001$). This indicated that although the bone structure had improved following treatment, elongation of the long bone was limited.

Insufficient mineralization and abnormal bone structure in transduced mice revealed by microcomputed tomography scans

A more detailed analysis of bone structure was next performed using microcomputed tomography (micro-CT). We first examined the therapeutic effects obtained through *in vivo* gene therapy on femur bone conformation. Micro-CT examination of the femurs of TNALP-D$_{10}$ mice ($n = 3$) at day 90 showed normal bone formation in the midshaft, whereas epiphysis bone conformation remained abnormal (cupping deformity of the epiphysis, lack of cortical bone, and irregular positioning of the trabecular bone) (Figure 4a).

Several micro architectural parameters were also assessed in the micro-CT analysis. As shown in Figure 4b, these indicated that the femurs from TNALP-D$_{10}$ mice ($n = 3$) experienced hypomineralization compared with those of WT mice ($n = 3$). Bone mineral density (BMD) and bone volume/tissue volume (BV/TV) values were significantly lower than those of WT mice (means ± SD, TNALP-D$_{10}$ versus WT; BMD, 401.7 ± 76.1 versus 705.6 ± 33.2 mg/cm^3; $P < 0.005$, BV/TV, 16.1 ± 1.13 versus $19.1 \pm 1.26\%$; $P < 0.05$). No significant differences between TNALP-D$_{10}$ and WT mice were detected in the other parameters measured by micro-CT analysis (means ± SD, TNALP-D$_{10}$ versus WT; trabecular number (Tb.N), 3.41 ± 0.48 versus 4.19 ± 0.93/mm; $P = 0.26$, -trabecular thickness (Tb.Th), 48.2 ± 9.63 versus 46.7 ± 7.19 μm; $P = 0.84$, trabecular separation (Tb.Sp), 249.2 ± 33.4 versus 199.7 ± 47.4 μm; $P = 0.21$). These results suggested that in TNALP-D$_{10}$ mice, the femurs epiphysis still showed hypomineralization and abnormal bone structure.

Low-level ALP activity and irregular chondrocyte arrangement in the bones of transduced mice

To perform histological analysis of chondrocyte arrangement, growth plates in the femurs of day 90 TNALP-D$_{10}$ mice ($n = 5$) or WT mice ($n = 5$) were subjected to alcian blue staining with nuclear fast red. As shown in Figure 5a, femurs of TNALP-D$_{10}$ mice exhibited abnormal chondrocyte proliferation and irregular arrangement of cells. Hematoxylin and eosin (H&E) staining also showed abnormal chondrocyte arrangement and degenerated osteoid-like tissue (Figure 5b).

To analyze the ALP distribution near the knee joints, ALP activity in the femurs was histologically detected using the fast blue staining system. Positive ALP activity was recognized as purple staining. In the femurs of WT mice, strong ALP activity was observed in the trabecular bone and on the periosteal surface. By contrast, no ALP signal was observed in the femurs of untreated *Akp2*$^{-/-}$ mice
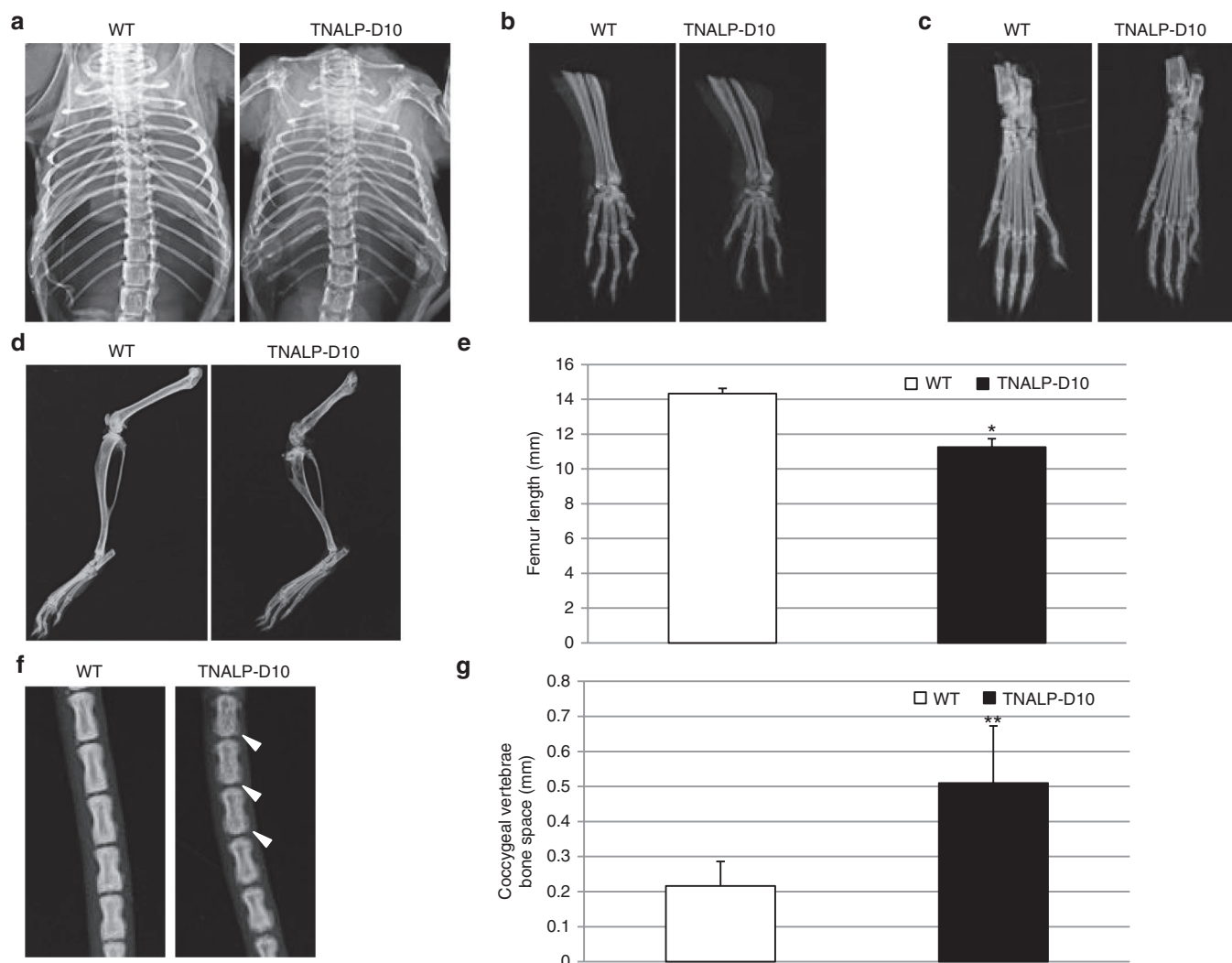
Figure 3 X-ray images of day 90 wild-type (WT) mice (*n* = 5) and TNALP-D$_{10}$ mice (*n* = 9). (**a**) Thorax, (**b**) forepaw, (**c**) foot, (**d**) hind limbs, (**e**) femur length (mm). Data represent the means ± SD. *P < 0.001. (**f**) Coccygeal vertebrae. Open triangles indicate the coccygeal vertebrae bone space. (**g**) Coccygeal vertebrae bone space. Data represent the means ± SD. **P < 0.01. TNALP-D$_{10}$, tissue-nonspecific alkaline phosphatase with deca-aspartates at the C-terminus.

(data not shown), which exhibited enlarged osteoid-like organization and abnormal chondrocyte proliferation (see Supplementary Figure S2b,c). In TNALP-D10 mice, however, low levels of ALP signal were observed in the growth plate and the outer periosteum (Figure 5c). This histological observation suggested that plasma ALP activity at 1 U/ml in the TNALP-D$_{10}$–transduced *Akp2*$^{-/-}$ mice was not sufficient to improve the abnormal bone structure of the femurs.

DISCUSSION

In this study, we demonstrated that scAAV8-MCK-TNALP-D$_{10}$–mediated muscle transduction enables sustained expression of TNALP-D$_{10}$, prolonged survival, and normal physical activities in lethal HPP model mice. Skeletal structure was significantly improved in the treated mice, however, limited elongation of the long bone and irregular chondrocytes arrangement were still observed as was hypomineralization compared with WT mice. Ectopic calcification was not detected. These results suggest that i.m. injection of scAAV8-MCK-TNALP-D$_{10}$ would be a safe and practical option to treat the severe infantile form of HPP.

We previously reported an effective therapeutic benefit using a single intravenous injection of recombinant adeno-associated virus 8 (AAV8) vector expressing TNALP-D$_{10}$ driven by the tissue nonspecific CAG promoter.[9] In this approach, the vector was introduced into systemic organs including heart, liver, lung, and muscle. The major concern, therefore, is the risk of inadvertent germ line gene transfer. The safety of systemic injection of viral vectors has not yet been established. As a safer and more practical approach, we examined the feasibility of AAV8-mediated, muscle-directed gene therapy. Skeletal muscle is an important candidate as a reservoir for vector-mediated ERT because of its large mass, easy accessibility, and high vascularity. The AAV vector is ideal for long-term gene expression in muscle tissues because it is nonintegrated but highly stable in nondividing muscle fibers. Long-term systemic delivery of therapeutic protein has been successfully achieved after direct i.m. injection of AAV vectors for the treatment of inherited lipoprotein lipase deficiency (LPLD),[12] hemophilia,[15] and muscular dystrophy.[11] Among its many serotypes, AAV1 and AAV8 are thought to be particularly useful for muscle-directed gene therapy.[12,16] Recently, i.m. injection of an AAV1 construct expressing LPL, alipogene tiparvovec (Glybera),
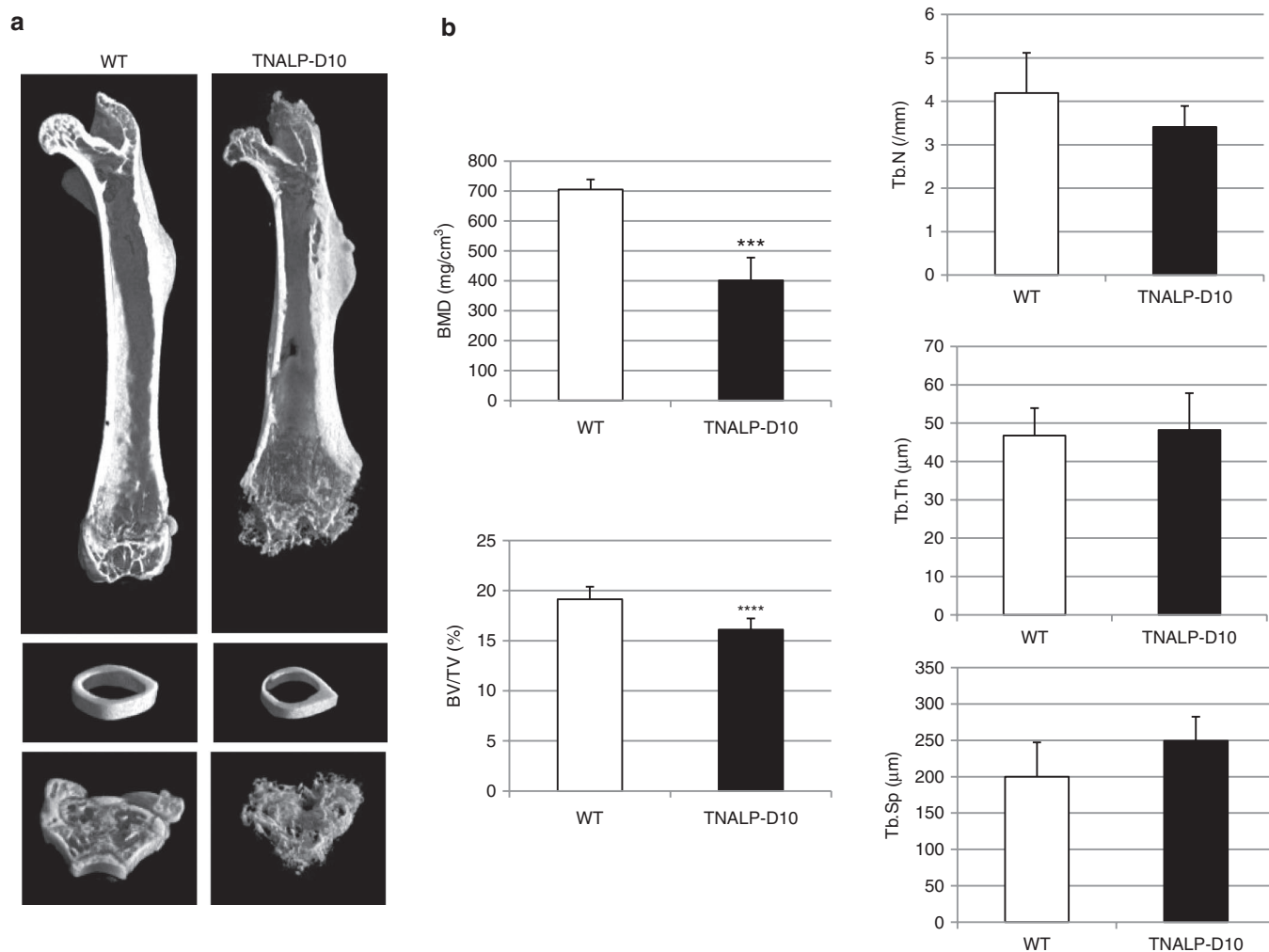
Targeted treatment of HPP via the MCK promoter
A Nakamura-Takahashi *et al*.

npg

5

Figure 4 Microcomputed tomography (micro-CT) reconstruction of the femur of wild-type (WT) mice (*n* = 3) and TNALP-D$_{10}$ (*n* = 3). (**a**) Micro-CT images of the entire femur (from top to bottom), the midshaft (center), and the epiphysis (bottom). (**b**) Morphometric evaluation of cancellous bone. The following parameters were determined: BMD, bone mineral density; BV/TV, bone volume/tissue volume; Tb.N, trabecular number; Tb.Th, trabecular thickness and Tb.Sp, trabecular separation. Data represent the means ± SD. ***$P < 0.005$. ****$P < 0.05$. TNALP-D$_{10}$, tissue-nonspecific alkaline phosphatase with deca-aspartates at the C-terminus.

was approved for treatment of LPLD by the European Medicines Agency as the first-approved gene therapy in the European Union. In this clinical protocol, Glybera is administered in a one-time series of up to 60 i.m. injections in the legs. AAV8 has been reported to be an even more efficient and safe vector for muscle-directed gene therapy with high levels of transgene expression and less immunogenicity.[17,18] Although AAV capsid–induced T-cell response might be a concern of vector administration at high dose, this response could be controlled by a short course of glucocorticoids in the clinical study with AAV8.[19] The utility of AAV8 in muscle-directed gene therapy has been studied in large animal models.[20]

To further enhance the safety of AAV vector–mediated ERT, we utilized a muscle-specific promoter instead of a tissue-nonspecific promoter with viral enhancer elements. The MCK promoter is a typical muscle-specific promoter, and its truncation form has been used for AAV-mediated, muscle-specific gene expression. In general, tissue-specific promoters are less active than are tissue-nonspecific promoters. To increase the level of gene expression in our study, we utilized a scAAV8 vector carrying the MCK promoter. scAAV provides rapid and highly efficient expression compared with that from conventional single-strand AAV vectors.[21,22] Direct

comparison of the MCK promoter and the CBA promoter in the AAV8 vector showed that the MCK promoter retained the ability to drive muscle-specific expression and that its promoter activity in C2C12 muscle-like cells was comparable with that of the CBA promoter. Furthermore, *in vivo*, the MCK promoter in the scAAV8 vector was effective in restricting the expression of EGFP to the skeletal muscle and heart, with expression in skeletal muscle higher than in the heart after i.m. injection with relatively higher expression in the skeletal muscle. These results confirmed the efficacy and specificity of muscle-directed transduction with the MCK promoter, in agreement with earlier studies.[23–25]

When mice were injected with 2.5×10^{12} v.g./body scAAV8-MCK-TNALP-D$_{10}$, the plasma ALP activities of treated mice increased significantly and were sustained at over 1 U/ml during the observation period (90 days after birth). In comparison with untreated *Akp2*$^{-/-}$ mice, which died within 3 weeks of birth, the life span of TNALP-D$_{10}$–treated mice was significantly prolonged. Furthermore, upon gross examination, the TNALP-D$_{10}$ mice exhibited normal physical activity and a healthy appearance. In addition, high ALP activity was restricted to the muscle (the target tissue). Although vector was detected at low levels in the heart and liver, no increases
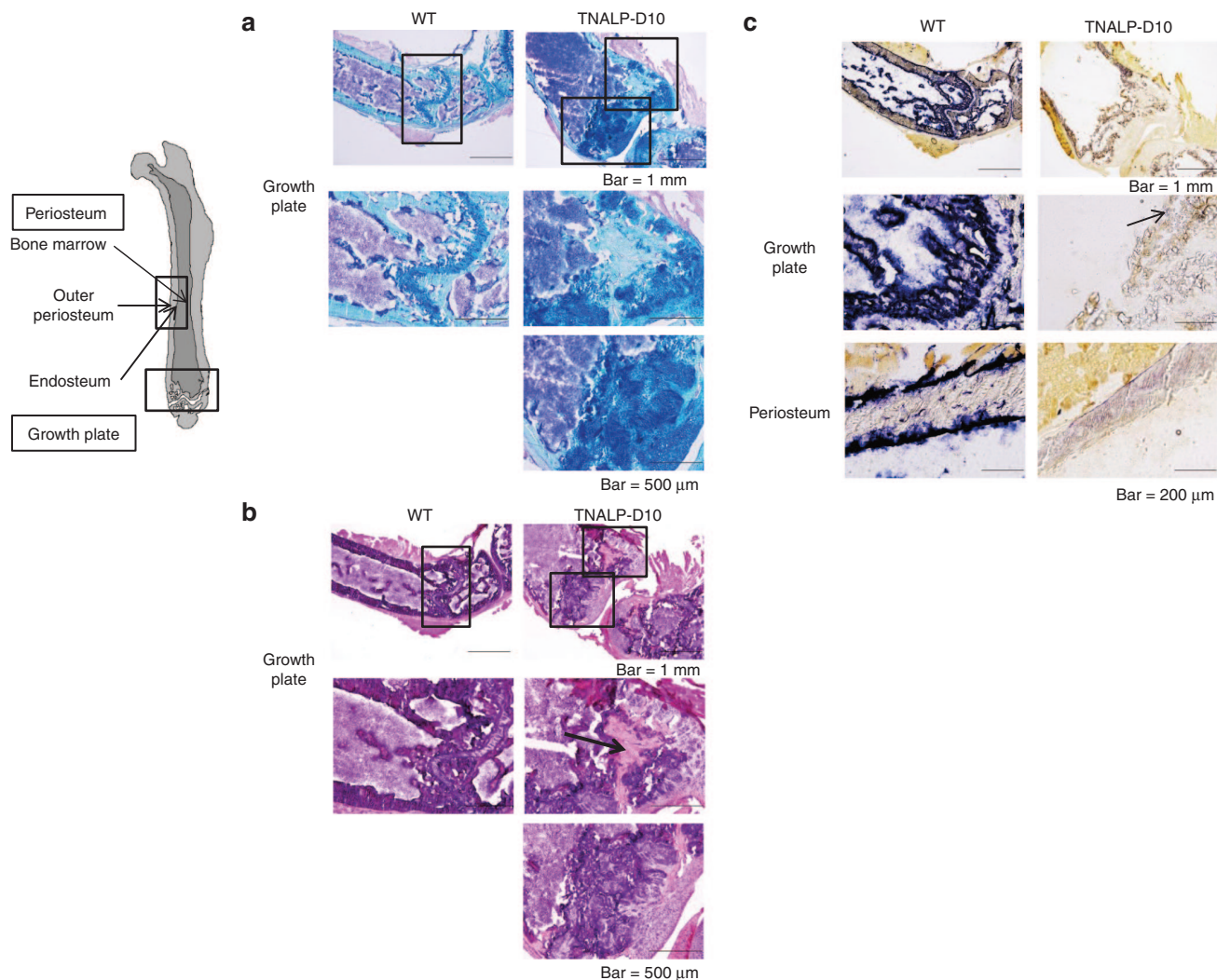
Figure 5 Femur schematic and representative pictures of alcian blue and ALP staining of the femurs of wild-type (WT) mice (left panels) and TNALP-D$_{10}$ mice (right panels). (**a**) Alcian blue staining with nuclear fast red of the femur growth plate (×4, bar =1 mm; ×10, bar = 500 µm). (**b**) Hematoxylin and eosin staining of the femur growth plate. The arrow indicates degenerated osteoid-like tissue (×4, bar = 1 mm; ×10, bar = 500 µm). (**c**) ALP staining in the quadrilateral area of the femur, growth plate, and the periosteum (×4, bar = 1 mm; ×20, bar = 200 µm). TNALP-D$_{10}$, tissue-nonspecific alkaline phosphatase with deca-aspartates at the C-terminus.

in ALP activity were detected in these tissues. Neither ectopic calcification nor other abnormal findings at the injected site were detected in the TNALP-D$_{10}$ mice (data not shown). These data indicate that i.m. injection of a scAAV8 vector carrying the MCK promoter can be used to achieve therapeutic levels of muscle-derived TNALP-D10 expression in neonatal HPP mice.

Conventional studies of bone structure by histochemical staining of ALP activity and X-ray imaging might not provide an accurate measure of the effects of gene therapy on bone structure. In the healthy skeleton, TNALP is present on the surface of the plasma membrane of osteoblasts and hypertrophic chondrocytes.[26] Accordingly, loss of TNALP function might influence chondrocyte formation and inhibit normal endochondral ossification. Therefore, we performed micro-CT analysis to examine the bone structure in detail. Compared with conventional X-ray images, micro-CT analysis utilizes arbitrary transected images to enable quantitative analysis of the trabecular bone. Although the use of micro-CT analysis has already been described in a previous report of ERT, our study is the first to use this method to confirm therapeutic effects on the femur bone through *in vivo* gene therapy.

The detailed structure of the short femur containing a blurred epiphysis could not be evaluated by conventional X-ray images. Micro-CT examination demonstrated normal formation of the midshaft but revealed hypomineralization and insufficient conformation of the trabecular bone in the epiphysis. Alcian blue staining of the femurs of TNALP-D$_{10}$ mice demonstrated inadequate chondrocyte proliferation, and ALP staining confirmed sporadic staining on the surface of the endosteal bone and spotty positive staining in the trabecular bone. Abnormal chondrocyte proliferation, which leads to the absence of cortical bone formation and abnormal architecture of the trabecular bone in the epiphysis, significantly retarded elongation of the long trunk bone in treated mice. This histological observation was consistent with the micro-CT examination. Thus, ALP activity at 1 U/ml plasma enabled prolonged survival and normal physical activities but was not sufficient to normalize bone structure and mineralization in *Akp2*$^{-/-}$ mice.

The markedly abnormal proliferation of chondrocytes observed in TNALP-D$_{10}$ mice appears to be characteristic of *Akp2*$^{-/-}$ mice, as a previously published study on ERT using soluble TNALP described similar findings in treated mice.[27] Such insufficient proliferation

could be induced by phosphate modulation of osteoblast and chondrocyte expression, differentiation, and function,[28–32] as well as induction of chondrocyte apoptosis.[33,34] In addition, feedback signaling from components of increased osteoid-like organization, up- or downregulation of bone mineralization factors, inflammatory factors, or microfracture and repair might also be involved in the etiology of this feature.[35] Therefore, improvement of the insufficient bone calcification and inadequate chondrocyte proliferation in patients with HPP remains challenging.

The objectives of future studies include the further enhancement of ALP activity to improve the degree of calcification in treated mice. For example, the MCK promoter used here could be replaced with more potent muscle-specific elements, such as spc5-12, CK8, and CK9.[36,37] Furthermore, early intervention such as prenatal gene therapy might be required to support normal differentiation of chondrocytes during fetal development. Additionally, when high doses of enzyme are infused continuously, antibodies against the ALP enzyme might be produced.[27] Therefore, it is of great importance to regulate the immune response in gene therapy studies to achieve maximum therapeutic benefit.

In conclusion, our results suggested that the Akp2^{−/−} mice could be effectively treated by a rAAV-mediated muscle TNALP-D$_{10}$ transduction. As a next stage of the study, further investigation with the use of immunosuppressive reagent or immune tolerance induction is expected to improve safety and therapeutic benefits. This approach with scAAV8-MCK-TNALP-D$_{10}$–mediated muscle transduction holds great promise for the treatment of the severe infantile form of HPP with appropriate strategies to regulate immune response.

MATERIALS AND METHODS

Plasmid construction and vector production
The recombinant scAAV vector plasmid, pscAAV-CB-EGFP, was a kind gift from Arun Srivastava, the University of Florida College of Medicine (Gainesville, FL). The self-complementary pscAAV-MCK-EGFP plasmid was generated by replacing the CBA promoter region[38] of pscAAV-CB-EGFP with the truncated MCK promoter region of pAAV-MCK-FLK[39] using the In-Fusion HD Cloning Kit (Clontech Laboratories, TaKaRa Bio Company, Ohtsu, Shiga, Japan). Similarly, the EGFP gene of pscAAV-MCK-EGFP was replaced with a bone-targeted, tissue-nonspecific ALP using the TNALP-D$_{10}$[9,13] sequence to obtain pdsAAV-MCK-TNALP-D$_{10}$. The recombinant scAAV8 vectors (scAAV8-CBA-EGFP, scAAV8-MCK-EGFP, and scAAV8-MCK-TNALP-D$_{10}$) were generated from cultured serum-free medium using polyethylenimine-based triple transfections of HEK293 cells.[40] The titer of each AAV vector was determined by real-time polymerase chain reaction (PCR) using a 7500 Fast Real-Time PCR Instrument (Applied Biosystems, Carlsbad, CA) with the primers for EGFP gene, forward, 5′-AGCAGCACGACTTCTTCAAGTCC-3′ and reverse, 5′-TGTAGTTGTACTCCAGCTTGTGCC-3′: for TNALP-D10 gene, forward, 5′-CCGTGGCAACTCTATCTTT-3′ and reverse, 5′-GAGACATTCTCTCGTTCACC-3′.

Animal procedures and vector injection
All animal procedures were performed in accordance with the guidelines approved by the Nippon Medical School Animal Ethics Committee. Akp2^{−/−} mice were obtained by mating Akp2^{+/−} mice with mice with a mixed genetic background of 129/J and C57BL/6J, which were generated by the Millán laboratory.[6] The mice were fed a rodent diet supplemented with pyridoxine (vitamin B$_6$) to suppress seizures.[41] Genotyping was performed by PCR with the primers forward, 5′-AGTCCGTGGGCATTGTGACTA-3′ and reverse, 5′-TGCTGCTCCACTCACGTCGAT-3′. To investigate muscle-directed transduction, the scAAV8-MCK-EGFP construct was injected into the bilateral quadriceps femoris muscle of newborn WT mice (day 1) at 5×10^{11} v.g./body diluted with phosphate-buffered saline (PBS) to a total volume of 15 µl. At 14 days after injection, the transduced mice were sacrificed under deep anesthesia by perfusion with 15 ml of PBS containing heparin (10 U/ml) followed by 15 ml of PBS and 5 ml of 4% paraformaldehyde phosphate buffer (4% PFA-PB). Samples were taken from the transduced quadriceps femoris muscle, heart,

liver, and kidney. To determine the expression of TNALP-D$_{10}$, scAVV8-MCK-TNALP-D$_{10}$ (2.5×10^{12} v.g./body diluted with PBS to a total volume of 15 µl) was injected into the bilateral quadriceps femoris muscle of neonatal Akp2^{−/−} mice on day 1. Physical activity and appearance were observed periodically. To analyze the therapeutic effects of scAAV8-MCK-TNALP-D$_{10}$ in the Akp2^{−/−} mice, treated mice were sacrificed at 90 days of age and perfused with 15 ml of PBS containing heparin (10 U/ml) followed by 15 ml of PBS. Samples were taken from the heart, liver, spleen, kidney, transduced quadriceps femoris muscle, genitalia, bone and bone marrow, and brain.

Spontaneous locomotor activity
Locomotor activity was measured in an open field of breeding gauge (24×14.5 cm) using a Smart video tracking system (Bio-Research Center, Tokyo, Japan) in a softly illuminated sound-proof room. At 30 days after birth, WT or TNALP-D$_{10}$ mice were put in a gauge. After 5 minutes of training, the movement that occurred for 20- to 30-second period in the gauge was measured three times using a video camera. The total distance (cm) traveled during a 1-minute period was estimated.

ALP activity in plasma and organs
Blood samples were collected from the orbital sinus using heparinized capillaries on days 30, 60, and 90 after birth. ALP activity in the plasma was quantified by a colorimetric assay for ALP activity, as described previously.[42] The ALP activity in 1 U was defined as the amount of enzyme needed to catalyze the production of 1 µmol p-nitrophenol per minute. The heart, liver, spleen, kidney, quadriceps femoris muscle, genitalia, tibial bone, and brain were each homogenized in 1 ml of distilled water using a Precellys 24 bead beater (Bertin Technologies, Paris, France) and centrifuged at 14,000g for 5 minutes. The ALP activity of the supernatant was analyzed as described previously and standardized per mg of protein. Protein concentrations were assayed using the DC protein assay kit (Bio-Rad, Hercules, CA).

Histochemical examination of bone
Removed knee joints were embedded in Super Cryoembedding Medium compound (Leica Microsystems, Wetzlar, Germany) and frozen without fixation or decalcification. Sections of 10-µm thickness were prepared by the Kawamoto film method (Leica Microsystems), air-dried for 5 minutes, fixed in 4% PFA-PB for 10 minutes, washed with PBS, and further washed with distilled water. Alcian blue staining with nuclear fast red, H&E staining, and ALP staining of the sections were performed. To analyze cartilage structure, sections were stained with alcian blue solution 8GX (pH 2.5) (Merck Millipore, Darmstadt, Germany) for 30 minutes, washed with distilled water for 2 minutes, and stained with 0.1% nuclear fast red solution (Merck Millipore) for 30 seconds. Standard H&E staining was performed for histological observation. ALP staining was conducted by incubating the tissue with naphthol AS-MX phosphate (0.1 mg/ml) and fast blue BB salt (0.6 mg/ml) in 20 ml of 0.1 M Tris-HCl buffer (pH 8.5) for 30 minutes at 37 °C, as described previously.[43] Sections were mounted on MAS-coated glass slides (Matsunami Glass, Tokyo, Japan) and examined under a light microscope. Sections were examined under a BX60 light microscope (Olympus, Tokyo, Japan).[42]

X-ray analysis
All radiographic images were obtained on µFX-1000 film (Fujifilm, Tokyo, Japan) with an energy level of 25 kV. Radiographs were exposed for 30 seconds and imaged with a Typhoon FLA-7000 scanner (Fujifilm). Femur length and coccygeal vertebrae bone spaces were measured in each image.

Micro-CT imaging
Micro-CT analysis was carried out using an HMX-225 Actis4 (Tesco, Houston, TX). Femurs were washed with PBS and scanned. Imaging conditions were as follows: matrix size, 512×512; tube voltage, 120 kV; tube current, 83 µA; magnification, ×15; slice pitch, 50 µm; voxel size, 23×23×50 (µm). The obtained digital image was processed to reconstruct three-dimensional (3D) images using reconstruction software (VG Studio; Volume Graphics, Heidelberg, Germany). The midshaft and epiphysis were selected as the scan sites (midshaft = half of the entire length; epiphysis = 1.5 mm above the lower edge).[44]

Morphometric evaluation of trabecular bone
Bone morphometry was performed using a 3D morphometry system (TRI/3D-BON; Ratoc, Tokyo, Japan) to determine BMD, BV/TV, Tb.N, Tb.Th, and Tb.Sp. The epiphysis region of interest was evaluated in a 0.5-mm thick region 0.5 mm above the growth plate.[44]

Biodistribution of the AAV vector

Genomic DNA was extracted from eight main organs (the heart, liver, spleen, kidney, quadriceps femoris muscle, genitalia, bone and bone marrow, and brain) of scAAV8-MCK-TNALP-D$_{10}$ i.m. injected mice, and homogenates were prepared using Precellys 24 bead beater. The samples were then centrifuged at 14,000g for 5 minutes. Genomic DNA was extracted from the tissue homogenates using the Gentra Puregene Kit (Qiagen Sciences, Germantown, MD) and subjected to real-time PCR to detect the copy number of the AAV vector. Genome copy titer was quantified by TaqMan real-time PCR (Applied Biosystems) using primers designed to amplify the TNALP-D10 gene (forward, 5′-CCGTGGCAACTCTATCTTT-3′; reverse, 5′-GAGACATTCTCTCGTTCACC-3′) and TaqMan probe (5′-TGCTGAGTGACACAGACAAGAA-3′). Oligonucleotide primers and TaqMan probes for the mouse transferrin receptor were purchased from Applied Biosystems and were used to quantify the amount of genomic DNA. Genomic DNA spiked with AAV vector plasmid DNA was used as the standard, and the average copy number per diploid was determined.

Statistical analyses

Data from *in vivo* and *in vitro* experiments were expressed as the means ± SD. Differences between groups were tested for statistical significance using the Student's t-test. P values less than 0.05 were considered statistically significant. The survival rate was determined by the Kaplan–Meier method, and differences in the survival rates were assessed by the log-rank test using Statcel 3 for Windows (OMS, Saitama, Japan).

REFERENCES

1. Rathbun, JC (1948). Hypophosphatasia: a new developmental anomaly. *Am J Dis Child* **75**: 822–831.
2. Millán, JL (2006). Alkaline phosphatases: structure, substrate specificity and functional relatedness to other members of a large superfamily of enzymes. *Purinergic Signal* **2**: 335–341.
3. Mornet, E (2007). Hypophosphatasia. *Orphanet J Rare Dis* **2**: 40.
4. Waymire, KG, Mahuren, JD, Jaje, JM, Guilarte, TR, Coburn, SP and MacGregor, GR (1995). Mice lacking tissue non-specific alkaline phosphatase die from seizures due to defective metabolism of vitamin B-6. *Nat Genet* **11**: 45–51.
5. Narisawa, S, Wennberg, C, and Millán, JL (2001). Abnormal vitamin B6 metabolism in alkaline phosphatase knock-out mice causes multiple abnormalities, but not the impaired bone mineralization. *J Pathol* **193**: 125–133.
6. Narisawa, S, Fröhlander, N and Millán, JL (1997). Inactivation of two mouse alkaline phosphatase genes and establishment of a model of infantile hypophosphatasia. *Dev Dyn* **208**: 432–446.
7. Millán, JL, Narisawa, S, Lemire, I, Loisel, TP, Boileau, G, Leonard, P *et al.* (2008). Enzyme replacement therapy for murine hypophosphatasia. *J Bone Miner Res* **23**: 777–787.
8. Aggarwal, SR (2014). A survey of breakthrough therapy designations. *Nat Biotechnol* **32**: 323–330.
9. Matsumoto, T, Miyake, K, Yamamoto, S, Orimo, H, Miyake, N, Odagaki, Y *et al.* (2011). Rescue of severe infantile hypophosphatasia mice by AAV-mediated sustained expression of soluble alkaline phosphatase. *Hum Gene Ther* **22**: 1355–1364.
10. Liu, YL, Mingozzi, F, Rodriguéz-Colôn, SM, Joseph, S, Dobrzynski, E, Suzuki, T *et al.* (2004). Therapeutic levels of factor IX expression using a muscle-specific promoter and adeno-associated virus serotype 1 vector. *Hum Gene Ther* **15**: 783–792.
11. Okada, T and Takeda, S (2013). Current challenges and future directions in recombinant AAV-mediated gene therapy of duchenne muscular dystrophy. *Pharmaceuticals (Basel)* **6**: 813–836.
12. Ferreira, V, Twisk, J, Kwikkers, K, Aronica, E, Brisson, D, Methot, J *et al.* (2014). Immune responses to intramuscular administration of alipogene tiparvovec (AAV1-LPL(S447X)) in a phase II clinical trial of lipoprotein lipase deficiency gene therapy. *Hum Gene Ther* **25**: 180–188.
13. Yamamoto, S, Orimo, H, Matsumoto, T, Iijima, O, Narisawa, S, Maeda, T *et al.* (2011). Prolonged survival and phenotypic correction of Akp2(-/-) hypophosphatasia mice by lentiviral gene therapy. *J Bone Miner Res* **26**: 135–142.
14. Sugano, H, Matsumoto, T, Miyake, K, Watanabe, A, Iijima, O, Migita, M *et al.* (2012). Successful gene therapy in utero for lethal murine hypophosphatasia. *Hum Gene Ther* **23**: 399–406.
15. Buchlis, G, Podsakoff, GM, Radu, A, Hawk, SM, Flake, AW, Mingozzi, F *et al.* (2012). Factor IX expression in skeletal muscle of a severe hemophilia B patient 10 years after AAV-mediated gene transfer. *Blood* **119**: 3038–3041.
16. Cimmino, G, Chen, W, Speidl, WS, Giannarelli, C, Ibanez, B, Fuster, V *et al.* (2009). Safe and sustained overexpression of functional apolipoprotein A-I/high-density lipoprotein in apolipoprotein A-I-null mice by muscular adeno-associated viral serotype 8 vector gene transfer. *J Cardiovasc Pharmacol* **54**: 405–411.
17. Franco, LM, Sun, B, Yang, X, Bird, A, Zhang, H, Schneider, A *et al.* (2005). Evasion of immune responses to introduced human acid alpha-glucosidase by liver-restricted expression in glycogen storage disease type II. *Mol Ther* **12**: 876–884.
18. Wang, L, Louboutin, JP, Bell, P, Greig, JA, Li, Y, Wu, D *et al.* (2011). Muscle-directed gene therapy for hemophilia B with more efficient and less immunogenic AAV vectors. *J Thromb Haemost* **9**: 2009–2019.
19. Nathwani, AC, Tuddenham, EG, Rangarajan, S, Rosales, C, McIntosh, J, Linch, DC *et al.* (2011). Adenovirus-associated virus vector-mediated gene transfer in hemophilia B. *N Engl J Med* **365**: 2357–2365.
20. Gao, GP, Alvira, MR, Wang, L, Calcedo, R, Johnston, J and Wilson, JM (2002). Novel adeno-associated viruses from rhesus monkeys as vectors for human gene therapy. *Proc Natl Acad Sci U S A* **99**: 11854–11859.
21. Wang, Z, Ma, HI, Li, J, Sun, L, Zhang, J and Xiao, X (2003). Rapid and highly efficient transduction by double-stranded adeno-associated virus vectors *in vitro* and *in vivo*. *Gene Ther* **10**: 2105–2111.
22. McCarty, DM, Fu, H, Monahan, PE, Toulson, CE, Naik, P and Samulski, RJ (2003). Adeno-associated virus terminal repeat (TR) mutant generates self-complementary vectors to overcome the rate-limiting step to transduction *in vivo*. *Gene Ther* **10**: 2112–2118.
23. Shield, MA, Haugen, HS, Clegg, CH and Hauschka, SD (1996). E-box sites and a proximal regulatory region of the muscle creatine kinase gene differentially regulate expression in diverse skeletal muscles and cardiac muscle of transgenic mice. *Mol Cell Biol* **16**: 5058–5068.
24. Sharma, M, Kambadur, R, Matthews, KG, Somers, WG, Devlin, GP, Conaglen, JV *et al.* (1999). Myostatin, a transforming growth factor-beta superfamily member, is expressed in heart muscle and is upregulated in cardiomyocytes after infarct. *J Cell Physiol* **180**: 1–9.
25. Reisz-Porszasz, S, Bhasin, S, Artaza, JN, Shen, R, Sinha-Hikim, I, Hogue, A *et al.* (2003). Lower skeletal muscle mass in male transgenic mice with muscle-specific overexpression of myostatin. *Am J Physiol Endocrinol Metab* **285**: E876–E888.
26. Orimo, H (2010). The mechanism of mineralization and the role of alkaline phosphatase in health and disease. *J Nippon Med Sch* **77**: 4–12.
27. Oikawa, H, Tomatsu, S, Haupt, B, Montaño, AM, Shimada, T and Sly, WS (2014). Enzyme replacement therapy on hypophosphatasia mouse model. *J Inherit Metab Dis* **37**: 309–317.
28. Beck, GR Jr, Zerler, B and Moran, E (2000). Phosphate is a specific signal for induction of osteopontin gene expression. *Proc Natl Acad Sci U S A* **97**: 8352–8357.
29. Giachelli, CM (2005). Inducers and inhibitors of biomineralization: lessons from pathological calcification. *Orthod Craniofac Res* **8**: 229–231.
30. Conrads, KA, Yi, M, Simpson, KA, Lucas, DA, Camalier, CE, Yu, LR *et al.* (2005). A combined proteome and microarray investigation of inorganic phosphate-induced pre-osteoblast cells. *Mol Cell Proteomics* **4**: 1284–1296.
31. Giachelli, CM (2003). Vascular calcification: *in vitro* evidence for the role of inorganic phosphate. *J Am Soc Nephrol* **14**(9 suppl. 4): S300–S304.
32. Terkeltaub, RA (2001). Inorganic pyrophosphate generation and disposition in pathophysiology. *Am J Physiol Cell Physiol* **281**: C1–C11.
33. Yadav, MC, Lemire, I, Leonard, P, Boileau, G, Blond, L, Beliveau, M *et al.* (2011). Dose response of bone-targeted enzyme replacement for murine hypophosphatasia. *Bone* **49**: 250–256.
34. Meleti, Z, Shapiro, IM and Adams, CS (2000). Inorganic phosphate induces apoptosis of osteoblast-like cells in culture. *Bone* **27**: 359–366.
35. Hough, TA, Polewski, M, Johnson, K, Cheeseman, M, Nolan, PM, Vizor, L *et al.* (2007). Novel mouse model of autosomal semidominant adult hypophosphatasia has a splice site mutation in the tissue nonspecific alkaline phosphatase gene Akp2. *J Bone Miner Res* **22**: 1397–1407.
36. Li, X, Eastman, EM, Schwartz, RJ and Draghia-Akli, R (1999). Synthetic muscle promoters: activities exceeding naturally occurring regulatory sequences. *Nat Biotechnol* **17**: 241–245.
37. Himeda, CL, Chen, X and Hauschka, SD (2011). Design and testing of regulatory cassettes for optimal activity in skeletal and cardiac muscles. *Methods Mol Biol* **709**: 3–19.
38. Yoshimura, M, Sakamoto, M, Ikemoto, M, Mochizuki, Y, Yuasa, K, Miyagoe-Suzuki, Y *et al.* (2004). AAV vector-mediated microdystrophin expression in a relatively small percentage of mdx myofibers improved the mdx phenotype. *Mol Ther* **10**: 821–828.
39. Isotani, M, Miyake, K, Miyake, N, Hirai, Y and Shimada, T (2011). Direct comparison of four adeno-associated virus serotypes in mediating the production of antiangiogenic proteins in mouse muscle. *Cancer Invest* **29**: 353–359.

40. Miyake, K, Miyake, N, Yamazaki, Y, Shimada, T and Hirai, Y (2012). Serotype-independent method of recombinant adeno-associated virus (AAV) vector production and purification. *J Nippon Med Sch* 2012; **79**: 394–402.

41. Négyessy, L, Xiao, J, Kántor, O, Kovács, GG, Palkovits, M, Dóczi, TP *et al.* (2011). Layer-specific activity of tissue non-specific alkaline phosphatase in the human neocortex. *Neuroscience* **172**: 406–418.

42. Sogabe, N, Oda, K, Nakamura, H, Orimo, H, Watanabe, H, Hosoi, T *et al.* (2008). Molecular effects of the tissue-nonspecific alkaline phosphatase gene polymorphism (787T > C) associated with bone mineral density. *Biomed Res* **29**: 213–219.

43. Sugiyama, O, Orimo, H, Suzuki, S, Yamashita, K, Ito, H and Shimada, T (2003). Bone formation following transplantation of genetically modified primary bone marrow stromal cells. *J Orthop Res* **21**: 630–637.

44. Noguchi, T, Matsunaga, S, Kinoshita, H, Fukuda, M, Saka, H, Ide, Y *et al.* (2013). A site-specific comparison of the trabecular structure in senescence-accelerated mice—evaluation of time-course changes in bone architecture using *in vivo* micro-CT. *J. Hard Tissue Biol* **22**: 171–176.

Supplementary Information accompanies this paper on the *Molecular Therapy—Methods & Clinical Development* website (http://www.nature.com/mtm)